High rate of mutation and efficient removal by selection of structural variants from natural populations of *Caenorhabditis elegans*

Ayush Shekhar Saxena[1,2] and Charles F. Baer[1,3]

1 – Department of Biology, University of Florida, Gainesville, FL, USA

2 – Present address – Regeneron Pharmaceuticals Inc., Tarrytown, NY, USA

3 – University of Florida Genetics Institute, Gainesville, FL, USA

Correspondence to:

Ayush Shekhar Saxena

ayushsaxena.iitg@gmail.com

Abstract

The importance of genomic structural variants (SVs) is well-appreciated, but much less is known about their mutational properties than of single nucleotide variants (SNVs) and short indels. The reason is simple: the longer the mutation, the less likely it will be covered by a single sequencing read, thus the harder it is to map unambiguously to a unique genomic location.

Here we report SV mutation rate estimates from six mutation accumulation (MA) lines from two strains of *C. elegans* (N2 and PB306) using long-read (PacBio) sequencing. The inferred SV mutation rate ~1/10 the SNV rate and ~1/4 the short indel rate. We identified 40 mutations, and removed 52 false positives (FP) by manual inspection of each SV call. Excluding one atypical line (5 mutations, 35 FPs), the signal (inferred mutant) to noise (FP) ratio is approximately 2:1. False negative rates were determined by simulating variants in the reference genome, and observing 'recall'. Recall rate ranges from >90% for short indels and declines as SV length increases. Small deletions have nearly the same recall rate as small insertions (~100bp), but deletions have higher recall rates than insertions as size increases. The reported SV mutation rate is likely an underestimate.

A quarter of identified SV mutations occur in SV hotspots that harbor pre-existing low complexity repeat variation. By comparison of the spectrum of spontaneous SVs to wild isolates, we infer that natural selection is not only efficient at removing SVs in exons, but also removes roughly half of SVs in intergenic regions.

Introduction

Based on the total number of bases affected, structural variants (SV) — large insertions and deletions, repeat expansions and contractions, inversions, and translocations — are the largest source of genetic diversity in the genomes of multicellular organisms, and they have the largest average phenotypic and fitness effects of any type of mutation (Collins et al. 2020; Beyter et al. 2021). SVs are associated with a host of human disorders, including autism (Marshall et al. 2008; Weiss et al. 2008; Pinto et al. 2010; Sanders et al. 2011), schizophrenia (Walsh et al. 2008; Karayiorgou et al. 2010), and several types of cancers (Friedman et al. 1994; Wooster et al. 1995; Meyerson and Pellman 2011; Stransky et al. 2014; Nattestad et al. 2018). The functional consequences of SVs are well-documented (Hurles et al. 2008; Conrad et al. 2010; Yi and Ju 2018).

In recent years, human population geneticists have converged on the idea that the genetic basis of complex disease can be largely accounted for by the combined influence of very rare, recently arisen variants of large effect (Wang et al. 2021) and variants of small effect at very many loci (the "omnigenome", Boyle et al. 2017). Both classes of variants imply a significant role for mutation, the former for obvious reasons and the latter because, even if the per-locus mutation rate is low, the cumulative genetic variance contributed by a large fraction of the genome at mutation-selection-drift balance may be non-trivial.

Given the outsized contribution of SVs to genetic diversity on the one hand, and the apparently important contribution of mutation to complex disease on the other, understanding the mutational properties of SVs is an important problem in biomedical genetics. More broadly, characterizing SV mutation is necessary for an unbiased estimate of the distribution of fitness effects (DFE) of new mutations, which is a longstanding goal of evolutionary genetics (Fisher 1922; Eyre-Walker and Keightley 2007). Nearly all estimates of the DFE are restricted to the effects of SNPs and small indels (and most are restricted to SNPs, e.g., Kousathanas and Keightley 2013; Kim et al. 2017; Tataru et al. 2017; Böndel et al. 2019; Gilbert et al. 2021; James et al. 2023; Crombie et al. 2024). Because SVs are

ignored, all the variation in fitness is ascribed to small indels and SNPs, artificially inflating their importance by an unknown amount that may be quite large.

The reason that the mutational properties of SVs are poorly characterized is not because their biological relevance is not appreciated; it obviously is. Rather, the problem is technical: SVs are challenging to unambiguously identify and characterize with short-read sequencing technology, which remains the dominant mode of whole-genome sequencing. Long-read sequencing is superior to short-read sequencing for SV calling for several reasons. Longer reads may span the entire region of interest in one contiguous molecule, including problematic regions such as low complexity repeats. Even when a single read does not span the entire region of interest, longer reads result in superior local *de novo* assemblies that can span regions much larger than the read length itself. The obvious disadvantages include cost and error rate with respect to base-substitution and small indel calls, although the accuracy of the latest generation of some long-read platforms approaches that of short-read sequencing (Harvey et al. 2023).

A complete *de novo* assembly (whole genome assembly, WGA) of an individual is the only method certain to capture the full array of structural variants in a genome (Chaisson et al. 2015). As the cost of long-read technology declines, genome assemblies from single individuals have become economically feasible. Audono et al. (2019) published fully assembled reference-quality genomes of 13 humans, from which they estimated genetic diversity resulting from SVs as a proof of concept. More recently, Nurk et al. (2022) employed long-read sequencing to finish a complete telomere-to-telomere sequence of a human genome. The application of long-read sequencing technology to characterize spontaneous mutations is still nascent, although it is evident that long-read sequencing picks up variants that are missed with short-read sequencing (Noyes et al. 2022; Lopez-Cortegano et al. 2023; Zhou et al. 2023; Hénault et al. 2024; López-Cortegano et al. 2025).

Here we present estimates of the spontaneous mutation rate and spectrum of SVs in a set of *C. elegans* mutation accumulation (MA) lines propagated under minimal selection for

88 ~250 generations. A schematic diagram of the MA experiment is depicted in **Figure 1**. Four
89 MA lines derived from the N2 strain and two MA lines derived from the PB306 strain, and
90 their ancestral progenitors, were sequenced using Pacific Biosciences Sequel and Sequel 2
91 technology. In addition, we report estimates of the standing SV diversity derived from long-
92 read sequences of the genomes of four wild isolates of *C. elegans*. Comparison of the
93 relative proportions of SVs to other variants (SNPs and small indels) among spontaneous
94 mutations to the same proportions in the standing variation provides an estimate of the
95 relative strength of selection against SVs in nature.

96 **Results**

97 *Workflow*

98 We identify structural variants (SVs), defined as mutations larger than 30 base pairs (bp),
99 using a combination of alignment and assembly, followed by conventional variant calling.
100 Recognizing the inherent challenges in SV detection, we attempted to automate the process
101 of discovering the optimal parameters for the variant calling pipeline using segregating SVs
102 as 'ground truth', under the assumption that a variant called across many wild isolates is
103 likely real. We discovered that the signal-to-noise ratio of spontaneous SVs is significantly
104 lower than that of segregating SVs, complicating the development of an appropriate pipeline.
105 These complications are detailed in section 2 of the **Supplementary Discussion**. We
106 ultimately adopted a workflow loosely based on the methodology of Audano et al. (2019),
107 with three key modifications:

108 1. Utilization of a superior aligner, **minimap2** (Li 2018), instead of **blasr**
109 (https://github.com/jcombs1/blasr);
110 2. Variant calling with **PBSV (**https://github.com/PacificBiosciences/pbsv); and, critically,
111 3. Manual ("by eye") verification of each SV call by inspection in **IGV** (Robinson et al.
112 2017).

113 This workflow involves aligning noisy PacBio raw reads ('subreads') to the *C. elegans*
114 reference genome, followed by *de novo* assembly of aligned reads in 60-kb tiles. The

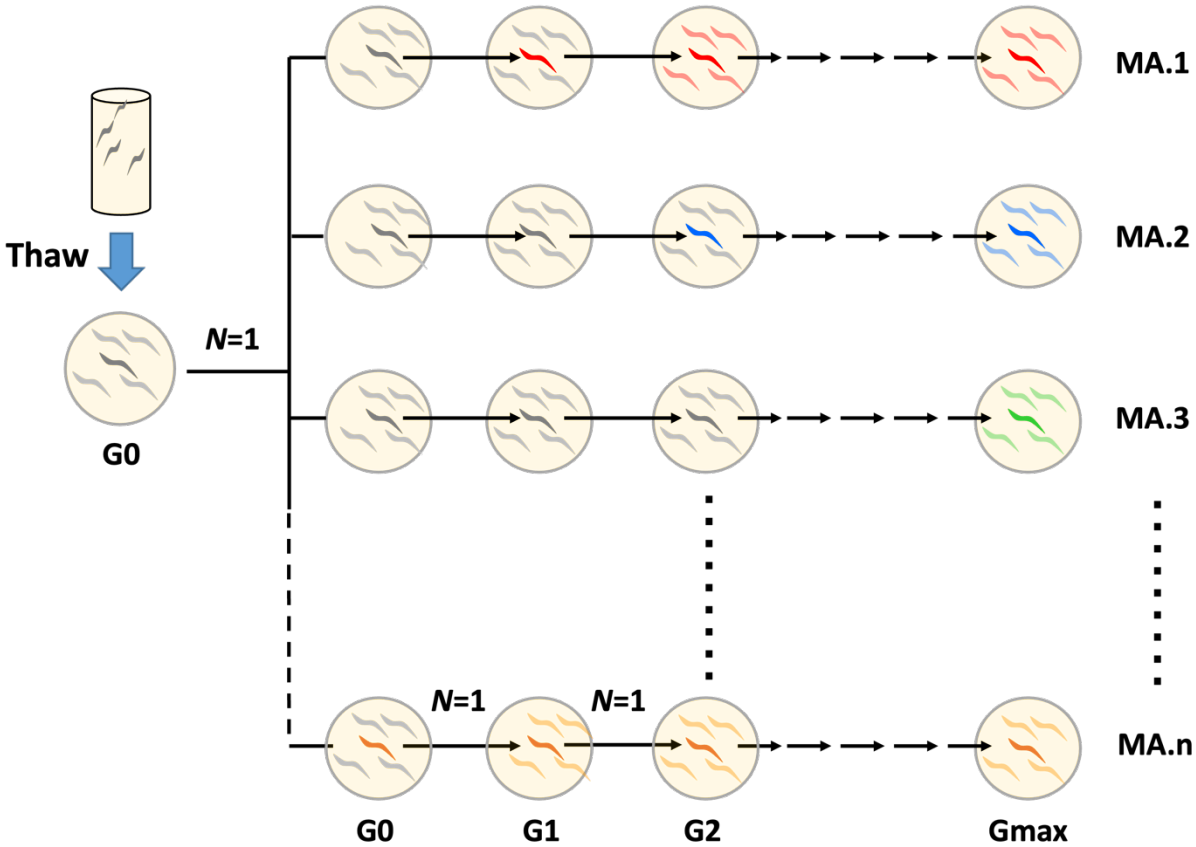

Figure 1. Schematic diagram of the mutation accumulation (MA) experiment. A cryopreserved sample of the ancestor (N2 or PB306) was thawed onto an agar plate (G0, left) and grown for a few days until the cryopreserved worms had reached the L4 larval stage. L4-stage worms were transferred singly to new NGM agar plates; those were the founders of the MA lines (MA.1, MA.2,...MA.n; n=100). At four-day intervals (one generation), a single immature worm was picked at random onto a new plate. This procedure was repeated until the experiment reached Gmax=250 generations. Individual MA lines experienced fewer than Gmax generations, G(ave)=238 generations. The different colored worms represent (the set of) unique mutations fixed in each MA line, which contribute to the among-line (mutational) variance.

assembled contigs —henceforth referred to as "pseudo-reads"— are then re-aligned to the reference genome, followed by conventional variant calling using PBSV. The pseudo-reads exhibit higher sequence quality than raw PacBio subreads, and aligned pseudo-reads are free from alignment errors that may occur with subread alignment. Accurate genotype calling in both the MA progenitor and the mutation accumulation (MA) line is required for

132 spontaneous SV calls, which increases the error rate of a spontaneous SV calling workflow
133 as opposed to a conventional SV calling workflow. Consequently, each final mutation call is
134 manually verified using IGV.

135 The summary of raw PacBio data is presented in **Supplementary Table 1**, which
136 includes the raw read error rate as well as the error rate of the assembly-generated pseudo-
137 reads. The error rate of raw reads, calculated from all N2-derived lines, is 14%, while the
138 pseudo-reads exhibit a significantly reduced error rate of 2.2%. The figures for other lines
139 are also available in **Supplementary Table 1**. Error rates were calculated after alignment
140 using the 'NM' tag in the BAM file, which represents the Levenshtein distance between the
141 aligned segment of the read and the reference. Notably, pseudo-reads also exhibit fewer
142 unaligned segments, measured as soft or hard clips after alignment. The percentage of
143 clipped bases upon alignment is approximately 5.3% for raw reads, compared to 4.3% for
144 pseudo-reads. To minimize the effect of reference bias on error rate estimates, we only
145 report results from N2-derived lines, from which the reference genome is derived, thereby
146 providing more reliable estimates. The gains to alignment quality are even higher for wild
147 isolates and PB306-derived MA lines.

148 Raw sequence data generated in this study are archived in the NCBI Short Read Archive
149 - PRJNA1233366. We also utilized publicly available long-read data of *C. elegans* wild
150 isolates from the following SRA repositories (PRJNA523481, and PRJNA1025857).

151

152 *SV mutation rate*

153 The SV mutation rate among observed SVs (i.e., not accounting for false negatives), is
154 estimated to be ~7 SVs per MA line, over approximately 238 generations per MA line, on
155 average. In comparison, we identified an average of 62 single nucleotide variants (SNV)
156 and 25 short indel mutations per line in the same set of lines. The inferred SV mutation rate
157 is roughly 10% of the SNV rate and ~30% of the short indel rate, indicating that SVs
158 comprise about 8% of new mutations, or roughly one new SV mutation per-genome every
159 ~30 generations. Summary statistics of SV mutations are presented in **Table 1**. The full set

Table 1. Summary statistics. Column headings: *Line* (strain.MA line # or wild isolate ID); *Type* (MA or Wild isolate); *#Muts* (number of inferred structural variants > 30bp in size); *Man. Corr* (# of SVs that required manual correction; see Methods for explanation); *#False pos.* (# of false positives); *%Recall (100 bp, 1Kb, 10Kb)* (% of simulated SVs of that length recalled; see Methods for explanation); *Ave. Cov*. (average sequencing coverage); *Raw error rate* (Error rate of raw PacBio subreads calculated after alignment to reference); *Pseudo-reads Error rate* (Error rate of assembled contigs after alignment to reference)*; #gens MA* (number of MA generations; see Methods); *Rel. fit (%)* (Fitness of MA lines relative to ancestor N2; unpublished data from Saxena et al.); #SNVs (number of base-substitution mutations); #Indels (number of indel mutations ≤ 30 bp). "Mutations" in wild isolates are variant compared to the N2 reference genome. For a more detailed discussion of false positives in wild isolates, see section 2 of Supplementary Discussion.

Line	Type	#Muts	Man. Corr	# False pos.	Recall rate (100-bp)	Recall rate (1 kb)	Recall rate (10 kb)	Ave. Cov.	Raw Error Rate (%)	Pseudo-read Error Rate (%)	#gens MA	Rel. Fit (%)	# SNVs	# Indels
MA517	N2 - MA	5	3	35	49	53	29	17	14	1%	242	72.6	53	17
MA530	N2 - MA	7	2	1	65	77	47	56	13	3%	243	122.2	51	26
MA563	N2 - MA	5	1	0	63	73	43	33	15	3%	237	66.0	70	24
MA566	N2 - MA	8	4	6	62	73	45	37	13	2%	238	58.6	71	21
MA445	PB306 - MA	10	5	6	57	68	42	50	16	6%	232	126.8	76	30
MA459	PB306 - MA	5	2	4	55	62	42	79	16	6%	235	61.4	61	31
PB306	WI	7691	-	-	59	69	43	188	15	7%	-	-	189278	73876
CB4856	WI	11028	-	-	56	65	37	59	18	7%	-	-	285787	104591
QX1211	WI	16528	-	-	50	49	30	54	18	8%	-	-	505065	164826
JU1088	WI	6181	-	-	60	69	39	52	17	6%	-	-	151734	61013
N2	Baer - N2	-	-	-	62	76	54	83	15	2%	-	-	-	-

169 of SVs and their attributes are given in **Supplementary Tables 2 and 3** for PB306 derived
170 lines and N2 derived lines respectively.
171
172 *Estimation of False Discovery Rates*
173 (*a*) False positives. The accuracy of SV mutation rate estimates is contingent upon the
174 accuracy of the variant calling workflow. False positives can be identified only by either (*i*)
175 "by eye" validation of putative variants using Integrative Genomics Viewer (IGV), or (*ii*) by
176 using a different sequencing technique, ideally by PCR amplification of the putative mutant
177 locus followed by Sanger sequencing of the resulting amplicon. However, those approaches
178 become impractical as the number of samples and/or putative variants increases.
179 We scrutinized each putative variant in the MA lines by visualizing the aligned
180 pseudo-reads, raw PacBio subreads, and Illumina reads from a separate study in IGV. We
181 identified 52 false positives in the original set of called putative SVs, resulting in a signal
182 (inferred mutant, n=40) to noise (false positive, n=52) ratio of 40/52 = 0.77. However, 2/3 of
183 the false positives occurred in one MA line (N2 line MA517). MA517 had lower sequencing
184 coverage than the other lines (17X vs 51X for other MA lines), which potentially introduced
185 alignment and/or assembly artifacts. When line MA517 is excluded, the signal-to-noise ratio
186 increases to ~2:1.
187 Among the true positive calls, minor corrections were made after visualizing the SVs
188 in IGV. Corrections are required when an MA SV occurs at a locus that already carries an
189 ancestral SV. Including other minor reasons for adjustments, corrections were necessary for
190 17 of the 40 true positive calls. The reasons for corrections are provided in **Supplementary**
191 **Tables 2 and 3**.
192 (*b*) False negatives. In contrast to identification of false positives, which must be done by
193 brute force, false negatives can be inferred by means of bioinformatics. We estimated the
194 false negative rate by (*i*) simulating SVs ("pseudo-variants") in the reference genome and (*ii*)
195 attempting to identify ("recall") the pseudo-variant in the sequenced sample. For example, a
196 pseudo-deletion introduced in the reference genome should appear as a variant pseudo-

197 insertion in the sequenced sample. We measured recall in both the MA lines and wild
198 isolates, with the latter providing information about the extent to which reference bias
199 impacts false negative rates.

200 Recall rates exceed 90% for short (~100-bp) indels and decline as SV length
201 increases, with deletions exhibiting higher recall rates than insertions (**Figure 2** and
202 **Supplementary Table S4**). Notably, recall rates were lower in wild isolates compared to the
203 N2 strain, presumably because the *C. elegans* reference genome is N2. As a result, slightly
204

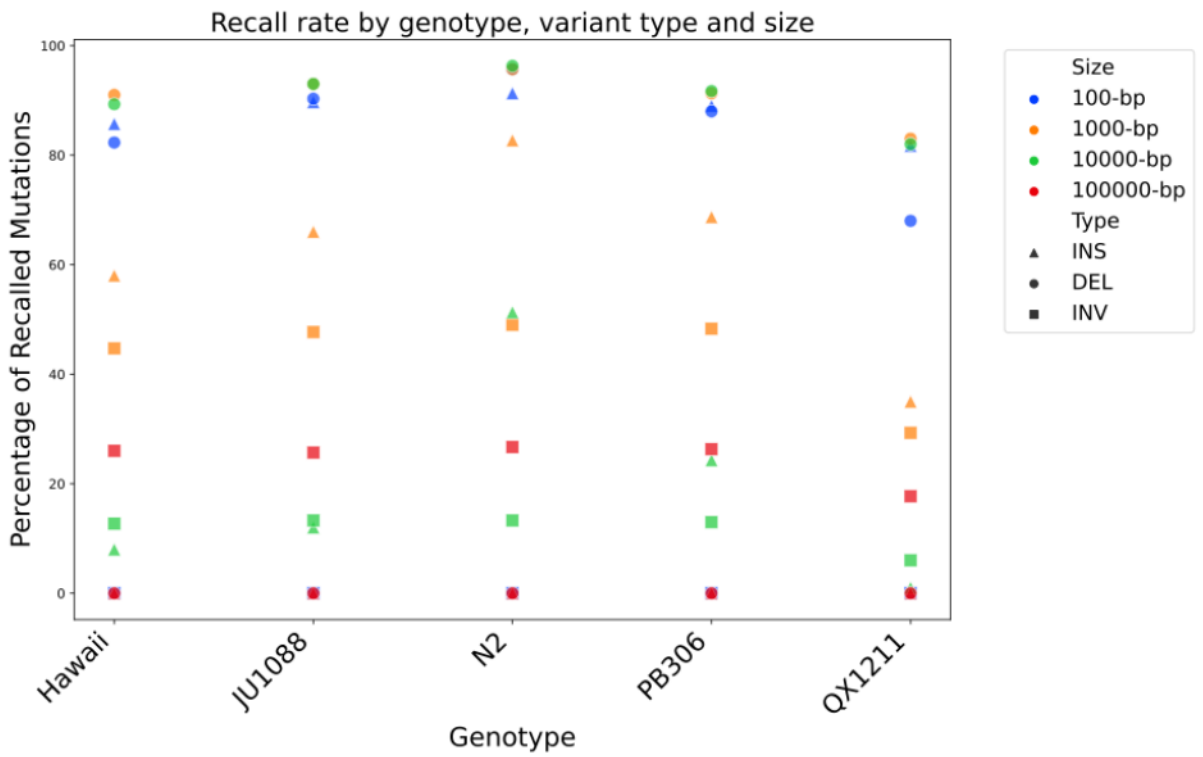

205

206 **Figure 2.** Recall rates by genotype, SV type, and SV size. N2 has the highest recall rate
207 across SV types and sizes. Small deletions (100 bp) have the highest recall rates, comparable
208 to 1-kb and 10-kb deletions. Recall rates of insertions drop sharply beyond 100 bp. Recall
209 rate decreases with increasing SV size and genetic divergence from N2, a trend also observed
210 in PB306-derived MA lines (not shown). Inversions have the lowest recall rates. QX1211, the
211 most divergent genotype from N2, is the most challenging for SV detection.
212

213 more SVs were missed in the PB306 MA lines than in the N2 MA lines (~4%). For reasons
214 that are unclear, we miss almost all small inversions (100-bp), whereas we are able to recall
215 roughly a quarter of 100-kb inversions.

SV mutation spectrum

Frequencies of SVs are listed by type and average size in **Table 2**. The total number of bases affected is approximately 16 kb in the four N2-derived lines, with a net loss of 1.5 kb across four lines (7 insertions and 18 deletions). For the two PB306-derived lines, approximately 15 kb of bases were affected in total, with a net

Table 2. SV spectrum by variant type and number of bases affected.

Line	Type	Insertions	Deletions	Inversions	Net bases affected	Net base gain (loss)
N2.517	MA	2	3	0	5,342	184
N2.530	MA	3	4	0	1,509	843
N2.563	MA	2	3	0	7,606	(309)
N2.566	MA	0	8	0	2,166	(2,166)
PB.445	MA	3	7	0	3,501	(1,397)
PB.459	MA	2	3	0	12,184	8,536
PB306	WI	4347	3280	64	4,027,284	1,791,544
CB4856	WI	5887	5056	85	5,205,431	1,562,847
QX1211	WI	9148	7279	101	7,949,707	2,849,281
JU1088	WI	3597	2525	59	3,331,096	1,465,676

gain of 7 kb (5 insertions and 10 deletions). Deletions outnumber insertions 2:1, the same bias observed among smaller indels in a larger set of N2 and PB306 MA lines (Rajaei et al. 2021). Among wild isolates, the number of insertions and deletions are nearly equal, with large insertions outnumbering large deletions by roughly 10% among SVs, and insertions and deletions being nearly equal among smaller indels. This suggests stronger purifying selection against deletions, on average, as opposed to insertions in the wild.

Spontaneous SV mutations are substantially larger in size compared to SVs identified in wild isolates (mean SV size: MA=1039 bp, wild=602 bp; median SV size: MA=404 bp, wild=125 bp; Kolmogorov-Smirnov test, $p<0.006$). This difference is primarily driven by the size of insertions (mean insertion size: MA=1574 bp, wild=799 bp; median insertion size: MA=840 bp, wild=162; K-S test, $p<0.004$), whereas deletions show no

237 significant difference in size (mean deletion size: MA=538 bp, wild=415 bp; median deletion
238 size: MA=131 bp, wild=105 bp; K-S test, p>0.21). Although the difference in deletion sizes is
239 not statistically significant, we observe a heavier tail in the size distribution of spontaneous
240 deletions, similar to spontaneous insertions. This distribution exhibits a multimodal pattern,
241 indicative of larger deletions in the MA lines (**Supplementary Figures S1-S3**).
242 A slight majority of spontaneous SVs (22/40) result from simple repeat expansions or
243 deletions, while four of the 40 SVs are associated with transposon-related events. The
244 average size of the repeat family across 22 independent events is 93 bp. In the PB306-
245 derived MA line 445, a CER1 transposon insertion was identified on chromosome 1,
246 resulting in an 8.8-kb insertion within a short 80-bp intron of the *smg-1* gene. The inserted
247 sequence contains 3' end of the *plg-1* gene and the full CER1 transposon sequence.
248 Similarly, in the N2-derived MA line 566, an RTE transposon insertion was observed, leading
249 to a 3.2-kb insertion at the 5' end of the *alg-1* gene. Additionally, seven of the 40 SVs are
250 located within hyperdivergent genomic regions, consistent with their frequency in the *C.*
251 *elegans* genome (~20%; Lee et al. 2021).
252
253 *Distribution of SVs across the genome*
254 The distribution of spontaneous SV mutations among exonic, intronic, and intergenic regions
255 does not deviate significantly from expectations based on genomic composition (Fisher
256 Exact test; chi squared statistic=1.89, df=2, sample size=140, p=0.39). Thus, the distribution
257 of spontaneous SVs reflects the relative proportion of the genome associated with those
258 regions.
259 In the wild isolates, the distribution of segregating SVs across the genome mirrors
260 the base-substitution distribution – higher in arms and lower in the centers (**Figure 3**); see
261 Figure 3 of Andersen et al. (2012) for the distribution of base-substitutions along *C. elegans*
262 chromosomes. The recombination rate is higher in chromosomal arms (of autosomes) than
263 centers in *C. elegans* (Rockman and Kruglyak 2009). The greater genetic diversity in
264 chromosomal arms is consistent with reduced Hill-Robertson interference in the arms

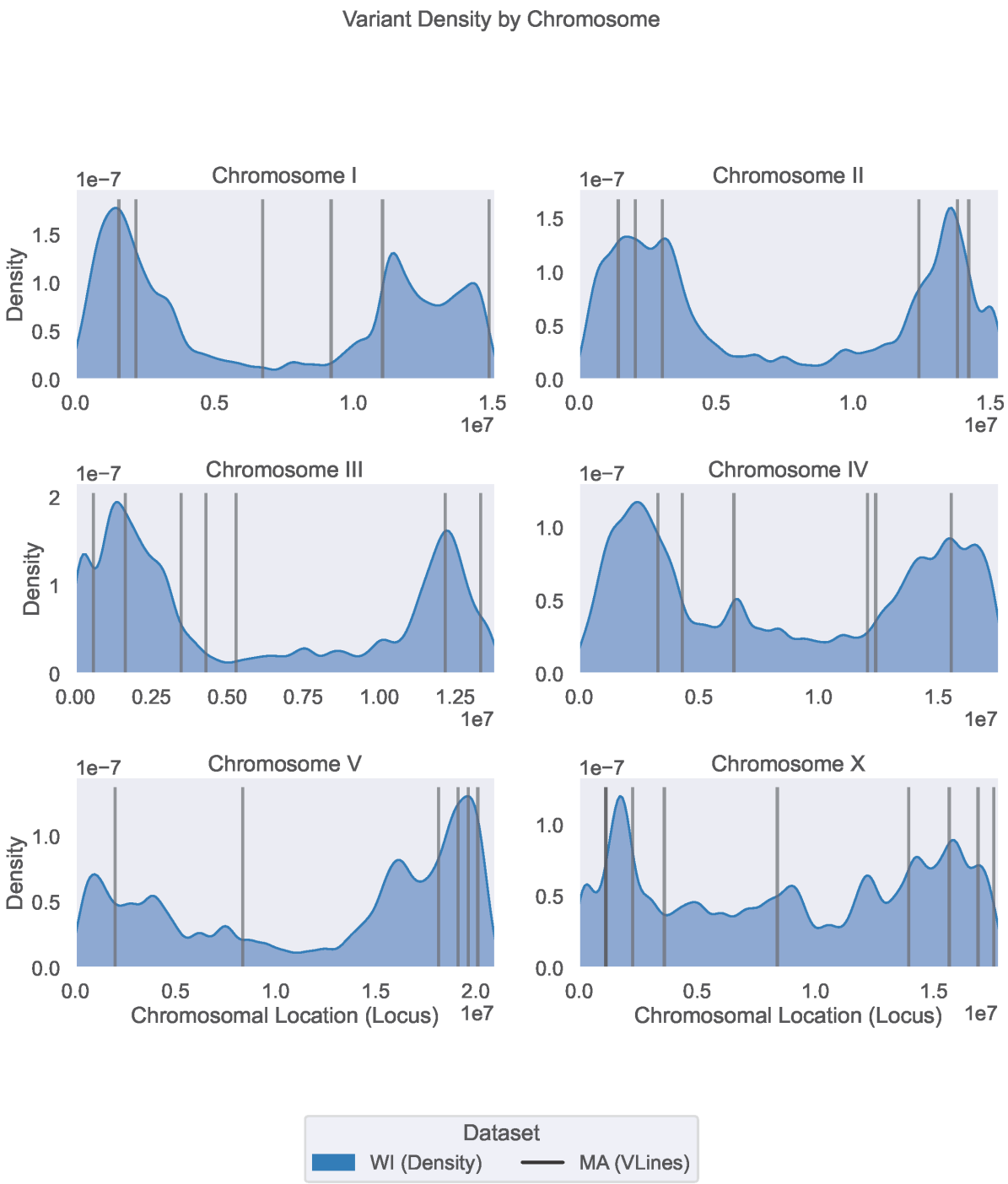

Figure 3. Distribution of SVs within and among chromosomes in wild isolates (density shown in blue) and MA lines (vertical black lines). The overall distributions between these two groups are not significantly different (Kolmogorov-Smirnov test; See text for details).

270 compared to the chromosome centers. We do not see this pattern on the X chromosome,
271 which is also consistent with expectation, since the recombination rate is nearly uniform on
272 the X.

273 It is possible, however, that the chromosomal distribution of genetic diversity is not
274 solely due to variation in the efficacy of purifying selection. It is possible that the SV
275 mutation rate may be higher in the arms. This view is supported by the fact that low
276 complexity DNA is overrepresented in the arms of *C. elegans* chromosomes (see
277 Supplementary Figures S4 and S5). Even with the small sample size of this study, we
278 observe more spontaneous SVs in the arms of the chromosomes than in the centers. A K-S
279 test revealed no significant deviation between the genomic distribution of spontaneous SVs
280 and those in the wild (p-values range from 0.29 to 0.92 across the six chromosomes). It may
281 be that the distribution of SVs across the genome can be explained by a combination of
282 mutation (more in the arms than the centers) and selection (stronger Hill-Robertson
283 interference in the centers).

284

285 *Fitness effects of SVs*

286 To infer the fitness effects of SVs, we compared the spectrum of spontaneous SVs
287 to that of wild isolates. Multiple aspects of the spectrum can be characterized – size,
288 type, location, etc. For example, spontaneous SVs are, on average, larger in size
289 compared to segregating SVs, aligning with the expectation that larger SVs are more
290 deleterious and are thus removed by natural selection. As noted, the deletion-to-
291 insertion ratio is higher among spontaneous SVs as opposed to segregating SVs,
292 implying that deletions are more deleterious than insertions, on average.
293 Functionally, the most important aspect of SV annotation is based on their genomic
294 location (e.g., exon, intron, intergenic). We analyzed nucleotide diversity across
295 different SV categories in MA lines and wild isolates, as well as among shorter

296 variants such as missense mutations and small indels, as shown in **Table 3.** SNVs in
297 introns, intergenic regions, and synonymous SNVs in exons were classified as
298 "neutral" base-substitution for this analysis. After normalizing for mutation rate, we
299 find that SV diversity in exons is approximately 14% of that of (putatively) neutral
300

301 **Table 3**. **Distribution of variant types by genomic context**. See text for details of
302 calculations of diversity measures.

Type	Context	Wild Isolates	PB306 MA	N2 MA	All MA	dN / dS*
SV	Exon	2866	4	6	10	0.14
	Intron	11818	5	14	19	0.31
	Intergenic	11292	6	5	11	0.52
SNV	Splice Variant	2840	2	1	3	0.48
	Disruptive Start/Stop Codon	1830	2	2	4	0.23
	Missense Variant	78191	11	30	41	0.96
	Intergenic Region	243014	53	88	141	Neutral
	Intron Variant	274542	52	94	146	Neutral
	Synonymous Variant	82326	6	8	14	Neutral
Indel	Frameshift Variant	8446	4	5	9	0.47
	In-frame Indel	2905	0	4	4	0.36
	Intergenic Region	74279	20	26	46	0.81
	Intron Variant	100183	32	45	77	0.65

303

304 base-substitutions, consistent with strong purifying selection (see Methods for details of the
305 calculation). This analysis is analogous to the dN/dS ratio as a test for selective constraint,
306 with the denominator (dS*) expanded to increase the sample size of MA variants. In
307 contrast to SVs in exons, the SNV diversity of missense mutations is ~96% of the neutral
308 expectation. This unexpectedly high frequency could be due to the sampling variance
309 associated with the small number of spontaneous mutations. Interestingly, SV diversity in
310 intergenic regions is ~52% of the neutral expectation, suggesting moderately strong
311 selection against SVs in these regions. This observation is, to our knowledge, the first of its
312 kind and warrants further investigation into the functional impacts of intergenic SVs, which

313 may have significant implications for human genetics research. We discuss the implications
314 of this result to the concept of 'junk DNA' later.
315
316 **Discussion**
317 *Limitations in Estimating the Contribution of Structural Variants to Fitness Decline*
318 Over the course of an average of 238 generations of mutation accumulation (MA), the six
319 MA lines in this study exhibited an average decline in absolute fitness of ~15% (Baer et al.
320 2006). Structural variants (SVs) constitute only ~7% of all detected variants. However,
321 accurately quantifying their contribution to fitness decline is challenging without detailed
322 knowledge of the distribution of fitness effects (DFE), which is likely influenced by factors
323 such as variant size and genomic context.
324 For instance, SVs occurring in exons represent a mutation class with particularly low
325 diversity in natural populations. After adjusting for differences in mutation rates across
326 variant classes, SV diversity in exons is approximately 14% of the neutral expectation, which
327 implies that selection removes 86 out of every 100 SV mutations that arise in an exon. Even
328 that is an underestimate, however, given that the standing variants potentially include
329 relatively new deleterious mutations that have persisted long enough to be observed but are
330 on their way to being selected out of the population (i.e. mutation-selection balance).
331 In contrast, small indels in introns, the most abundant non-neutral mutation class in
332 our dataset, exhibit diversity at ~65% of the neutral expectation, implying that selection
333 removes 35 out of every 100 introduced mutations in this category. Despite this, the MA
334 lines contain approximately eight times as many small indels in introns than SVs in exons.
335 While it is difficult to estimate relative selection coefficients (s) for these two classes without
336 a well-characterized DFE, their relative abundance suggests that small indels in introns
337 could contribute substantially to fitness decline, even if their average effect is weaker than
338 that of SVs in exons. Ignoring variant frequency in favor of a focus on average effects risks
339 underestimating the evolutionary consequences of more frequent but potentially less
340 deleterious mutations, such as small indels.

341

342 *Structural Variants in Low-Complexity Mutational Hotspots*

343 A significant proportion (~22.5%; 9 out of 40) of structural variants (SVs) identified in
344 mutation accumulation (MA) lines occur in low-complexity mutational hotspots. Previously,
345 Konrad et al. (2018) reported a similar estimate (~31%) for duplications and a much higher
346 estimate (~81%) for deletions occurring in loci with pre-existing CNVs in the ancestor, based
347 on short read sequencing of N2-dervied MA lines in *C. elegans*. Among the SV calls in MA
348 lines, the majority (22 out of 40) are simple repeat expansions or deletions. These
349 annotations were determined through manual inspection of variants using the JBrowse
350 genome browser as well as IGV rather than automated annotation, which, while scalable,
351 may introduce noise. The repeating units range in size from as small as dinucleotide
352 repeats (e.g., AT, CA, CT) to larger structural events, such as the deletion of a single copy
353 within a four-copy 360-mer repeat.

354 An unexpected observation is that 9 of the 22 SVs identified in repeat-rich regions
355 required a 'manual correction' due to a common misclassification in the workflow – where
356 the MA variant call occurs on a locus with a pre-existing variant in the ancestor. This
357 suggests that these loci represent mutational hotspots. Notably, the variant caller PBSV did
358 not correctly handle these cases, even in joint genotyping mode. **Supplementary Tables**
359 **S2 and S3** provide annotations for SV calls in MA lines, detailing the necessary corrections
360 following manual verification using IGV and genome browser inspection.

361 For example, a variant call on chromosome I of PB306-derived MA line MA445 (I:
362 1567493), illustrated in **Figure 4a** with a pedigree and **4b** with an IGV snapshot highlights
363 this issue. In the PB306 ancestor, this region contains a 3.1 kb insertion composed of
364 perfectly repeating copies of a 173-mer interspersed with additional sequence. Some of this
365 additional sequence contains similar repeating motifs, but of smaller units, and precise
366 annotation is difficult due to sequencing errors. The sequence of this insertion, along with its
367 repeating unit, is provided in **Supplementary Sequence File S1** in FASTA format. We
368 show the alignment of raw PacBio reads in **Supplementary Figure S6** and show the

369 **(a)**

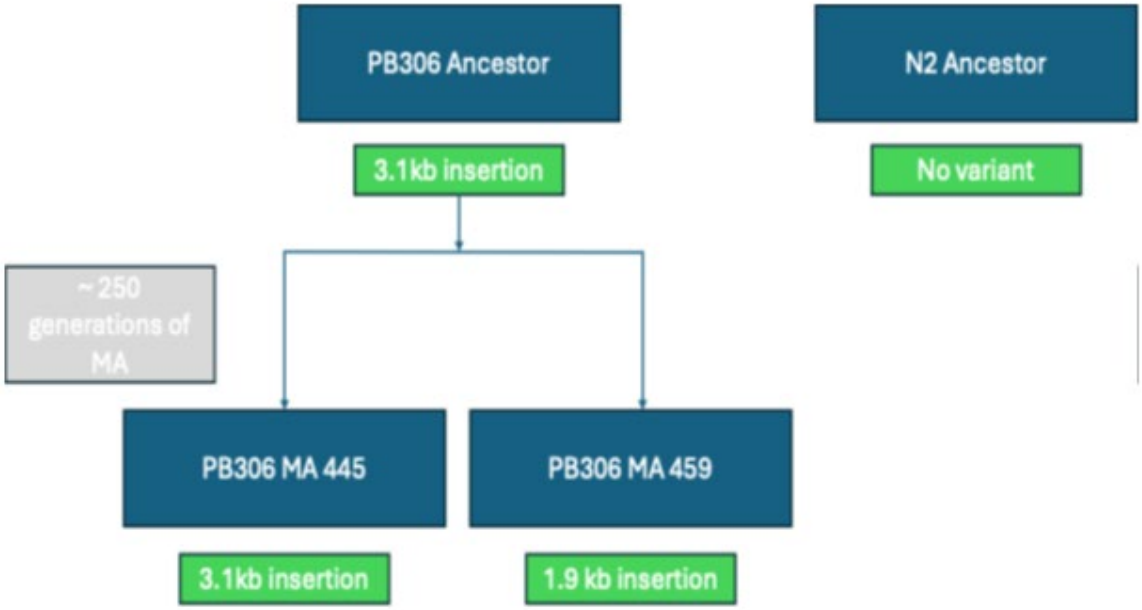

370

371 **(b)**

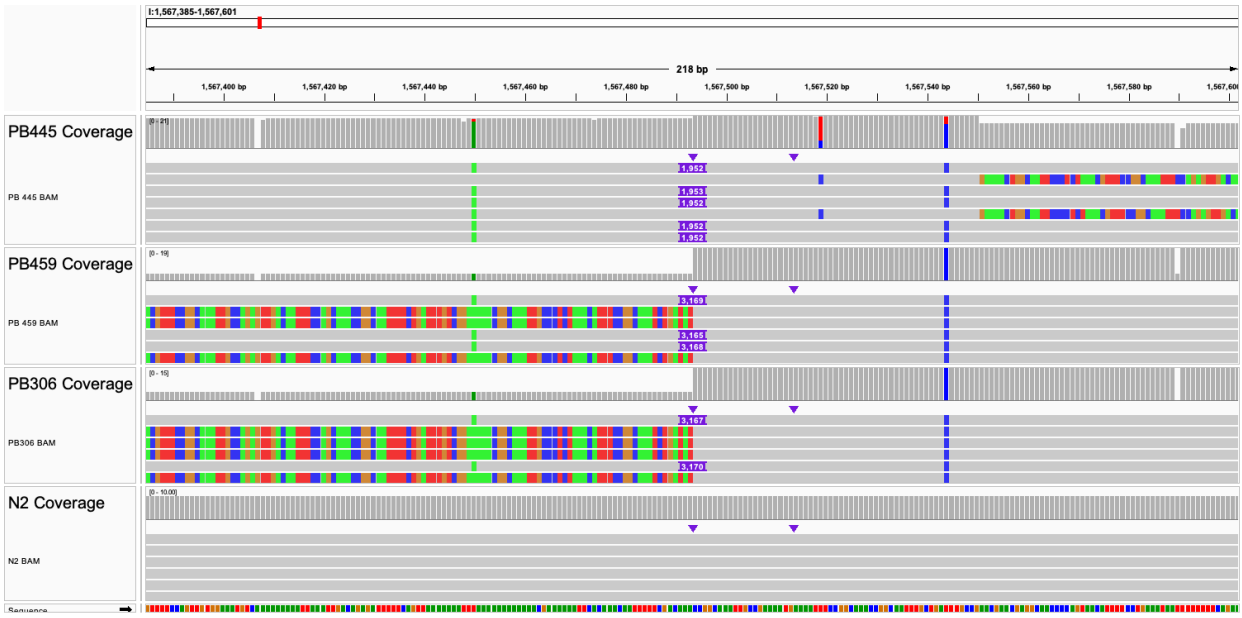

372

373 **Figure 4**. (**a**) A schematic representation of the variants identified at the locus (I: 1567493) in
374 the pedigree of MA lines. PBSV initially classified the 1.9 kb insertion and the 3.1 kb
375 insertion as two independent mutations. However, a deeper analysis—accounting for
376 sequencing errors—reveals that a 1.2 kb segment was deleted within the inserted sequence in
377 the ancestor, leading to the observed 1.9 kb insertion. (**b**) IGV snapshot of the 1.2 kb deletion
378 in PB306-derived MA 445. The IGV snapshot shows pseudo-read alignments, which are
379 assembled contigs representing longer sequences. Some pseudo-reads fail to fully capture the

380 inserted segment and appear as soft-clipped sequences. If the inserted segment is not entirely
381 covered within the pseudo-read, it is clipped from the alignment, appearing as base calls
382 (colored bars) instead of clean (gray bars), fully aligned sequences. Some insertion
383 sequences are misaligned because of the repetitive nature of the locus; however, all pseudo-
384 reads carry the insertion. Supplementary Figure S6 presents the same analysis using error-
385 prone PacBio raw reads.
386
387 repeating copies of 173-mer highlighted in text in **Supplementary Figure S7**. The same 3.1
388 kb insertion is also present in the PB306-derived MA line MA459, consistent with the
389 expectation that a variant present in the ancestor is inherited by its descendant. This
390 insertion is absent in the N2 ancestor, indicating that it is polymorphic in *C. elegans*.
391 Interestingly, in MA445, this region harbors a 1.9 kb insertion, effectively representing a 1.2
392 kb deletion relative to the PB306 ancestor. However, variant calling software failed to
393 annotate this as a deletion event, necessitating extensive manual validation of both raw and
394 assembled reads. Because some repeat copies are perfectly conserved while others exhibit
395 minor variations, the identification of this type of event remains beyond the resolution of
396 current variant calling algorithms.
397 The need for manual correction in 9 out of 22 repeat-associated SVs raises an
398 important question: Are certain repeat regions disproportionately prone to structural
399 variation? The *C. elegans* genome contains a vast number of repeat-associated sequences,
400 with 116,921 entries for repeat regions in the WS270 GFF3 annotations. Our findings
401 suggest that loci already carrying an SV in the ancestor are prone to recurrent SVs, making
402 them significant hotspots for genetic variation. Furthermore, these regions are likely
403 underrepresented or misannotated by automated variant calling pipelines. With only 9 such
404 identified events, it is beyond the scope of this study to understand the factors that cause
405 some repeat sequences to be hotspots. Notably, 2 of the 9 manually corrected repeat-
406 associated SVs occur in hyperdivergent regions—an observation worth noting, though we
407 refrain from drawing broader conclusions.
408

409 *SV Mutation Rate and Genome Size*

410 Genome size increased in five of the six MA lines assayed, by an average of ~1000 bp over
411 ~238 generations (~4bp/generation). Comparison of the estimate of the increase in genome
412 size by mutation with variation in genome size estimated from the wild isolates allows us to
413 estimate the strength of selection acting on genome size. If genome size is considered to be
414 a quantitative trait under selection (directional or stabilizing), at mutation-selection balance
415 (MSB), the ratio of the mutational variance (V_M) to the standing genetic variance (V_G) is
416 approximately equal to the strength of selection acting on a mutation that affects the trait
417 (Barton 1990; Kondrashov and Turelli 1992). Alternatively, if the trait of interest is a neutral
418 trait at mutation drift equilibrium (MDE), in a predominantly selfing population (such as *C.*
419 *elegans*) $V_G \approx 4N_eV_M$, where N_e is the effective population size (Lynch and Hill 1986; Denver
420 et al. 2005). The ratio of V_G to V_M for genome size is ~27000, which implies a selection
421 coefficient $s \approx 3.7 \times 10^{-5}$. If we assume the demarcation of effective neutrality is $4N_es<1$
422 (Kimura 1962; Kondrashov et al. 2006) and that N_e of *C. elegans* is on the order of 10^5
423 (Gilbert et al. 2021), it is plausible that genome size is under weak, but effective selection,
424 with the obvious caveat that any measure of variance estimated from a sample of fewer than
425 ten genomes is not robust.

426

427 *Estimating the Fraction of the Genome under Evolutionary Constraint*

428 We observe that selection efficiently removes most SVs, regardless of their genomic
429 locations (genic versus intergenic). This finding challenges the conventional view of "junk
430 DNA," which is often assumed to evolve free from the constraints of purifying selection. Our
431 results suggest that a larger fraction of the genome may be functionally relevant than
432 previously inferred from studies focusing on base substitutions. Unconstrained genomic
433 regions are typically defined by the absence of purifying selection. However, it is possible
434 that some genomic regions can tolerate base substitutions but not SVs. For instance,
435 consider a hypothetical low-complexity region between an enhancer and a promoter
436 (Bateman and Johnson 2022). Base substitutions in such regions may not disrupt gene

437 function, whereas SVs that alter the distance between the enhancer and promoter might,
438 which could in turn negatively impact fitness. Similarly, regulatory sequences flanking genes
439 may be more tolerant of base substitutions than of small indels or larger SVs. In a similar
440 vein, Payer et al. (2017) found that polymorphic *Alu* elements in the human genome were
441 significantly associated with Trait Associated SNPs (TASs) in human GWAS. Larger-scale
442 studies, capable of identifying more SV mutations, could reveal many such regions that
443 appear to evolve freely based on SNP variation but are subject to purifying selection against
444 SVs.
445
446 *Implications for GWAS*
447 Our findings have significant implications for genome-wide association studies (GWAS),
448 which typically rely on exome sequencing data and the analysis of short variants such as
449 single-nucleotide variants (SNVs) and small indels. While this approach has been highly
450 successful in identifying genetic variants associated with numerous traits and diseases, our
451 results highlight a potential blind spot in the detection and interpretation of structural variants
452 (SVs), particularly those in noncoding regions such as intergenic areas. Specifically, we
453 observed that SVs in exons are under strong purifying selection, with diversity reduced to
454 14% of the expected value after accounting for mutation rates. This underscores the
455 functional importance of exonic SVs and aligns with the focus on exome sequencing in
456 GWAS.
457 However, our finding that intergenic SV diversity is reduced to 52% of the expected
458 value suggests that many of these variants are also functionally significant, likely due to their
459 impact on regulatory elements or chromatin structure. This is in contrast to the relatively
460 weaker selection observed for missense SNVs, which retain 96% of their expected diversity.
461 The data reveal a striking contrast in the selective pressures acting on different classes of
462 mutations. Variants that strongly disrupt gene function—such as splice site mutations,
463 frameshifts, and structural variants in coding regions—exhibit significantly reduced diversity
464 in the wild, suggesting that purifying selection effectively removes them from the population.

465 In contrast, missense mutations, which alter protein structure but do not necessarily abolish
466 function, persist at much higher frequencies. The accumulation of mildly deleterious
467 mutations could also contribute, in the long run, to compensatory adaptation via the
468 introduction of variants of small positive effects.

469 These observations raise critical questions about the extent to which current GWAS
470 approaches may overlook the contributions of intergenic SVs to phenotypic variation and
471 disease. Expanding the scope of GWAS to include comprehensive SV profiling, particularly
472 in noncoding regions, may uncover a substantial reservoir of previously unrecognized
473 genetic contributors to human health and disease.

474

475 **Conclusion**

476 The spontaneous SV mutation rate is inferred to be approximately 8% of the SNV/small indel
477 rate, but that is likely an underestimate. SVs are efficiently removed from natural
478 populations, indirectly implying a function (biochemical or otherwise) to a larger fraction of
479 the genome than is typically assumed.

480

481 **Material and Methods**

482 *MA Protocol*

483 The MA protocol has been described in detail previously (Baer et al. 2005) and is depicted in
484 **Figure 1**. The method by which we estimated the number of generations of MA for a line
485 (below Gmax) is reported in Saxena et al. (2019).

486

487 *DNA extraction, library preparation, and sequencing*

488 Cryopreserved samples of the MA lines were thawed onto 100 mm NGMA agar plates
489 seeded with a lawn of *E. coli* OP50 and grown for 2-3 days, until there were many gravid
490 worms, at which time worms were harvested, "bleached" to remove bacterial and fungal
491 contamination (Stiernagle 2006), and embryos transferred to a new, seeded 100 mm plate.
492 L1 larvae were collected the next day and transferred to seven seeded 100 mm plates and

493 grown until the plates were nearly starved. Worms were washed from the plates, double-
494 rinsed in M9 buffer, and pelleted for DNA extraction. DNA was extracted from each sample
495 with the Quiagen Gentra Puregene kit, following the manufacturer's instructions. Extracted
496 DNA samples were sent to the University of Maryland genomics core facility for library
497 preparation and sequencing on the Pacific Biosciences Sequel platform.
498
499 *Variant Calling Pipeline*
500 We evaluated multiple variant calling strategies, including direct alignment-based
501 approaches and de novo assembly followed by genome-to-genome alignment using
502 Assemblytics (Nattestad and Schatz 2016). Ultimately, we adopted a modified version of the
503 SMRT-SV2 (Audano et al. 2019) pipeline, as it provided a balance between sensitivity and
504 specificity while minimizing false positives. A detailed discussion of our rationale for
505 selecting this approach over others is provided in section 1 of the **Supplementary**
506 **Discussion**.
507 The SMRT-SV2 pipeline processes noisy PacBio subreads by aligning them to the
508 reference genome using blasr (Chaisson and Tesler 2012). These alignments are then
509 segmented into 60-kb tiles, which are assembled using Canu (Koren et al. 2017). This
510 localized assembly approach reduces interference from reads originating from other
511 genomic regions. Importantly, the assembled contigs effectively "clean" the PacBio
512 subreads, leading to improved downstream alignments. While SMRT-SV2 automatically re-
513 aligns these contigs using blasr, we opted to replace blasr with minimap2 (Li 2018), which
514 provided superior alignment performance for our dataset.
515 SMRT-SV2 includes its own variant caller. However, it led to an unacceptably high
516 false positive rate for de novo mutations. To improve accuracy, we benchmarked several
517 alternative structural variant (SV) callers, including Sniffles (Sedlazeck et al. 2018) and
518 PBSV (Wenger et al. 2019), ultimately selecting PBSV due to its optimized performance on
519 high-quality PacBio reads. Further details on the performance of SMRT-SV2, Sniffles, and
520 SMRT-SV2 variant calling are provided in section 3 of the **Supplementary Discussion**.

521 In cases where a potential variant was detected, SMRT-SV2 produced multiple
522 assemblies—referred to as “pseudo-reads”—for the candidate locus. These pseudo-reads
523 were then aligned with minimap2 and variants were called using PBSV. Despite this
524 refinement, we still observed many false positives, albeit a manageable number, further
525 necessitating manual curation. Each candidate variant was inspected in IGV (Robinson et
526 al. 2017) and JBrowse genome browser (Diesh et al. 2023), comparing error-prone raw
527 PacBio subread alignments, pseudo-read alignments, and independent Illumina sequencing
528 data generated for a separate study. Only variants present in the mutation accumulation
529 (MA) line but absent in both the MA ancestor and other MA lines were considered true de
530 novo mutations. Once validated, variants were functionally annotated using genome
531 browser annotations to classify their genomic context (e.g., exon, intron, UTR, repetitive
532 element, hyperdivergent region, potential regulatory elements).
533 For identifying segregating SVs, we followed the same pipeline with one key
534 difference: instead of an ancestor-descendant comparison, all wild isolates were jointly
535 called using PBSV.
536
537 *Variant Annotation*
538 Annotation of structural variants (SVs) identified in the mutation accumulation (MA) lines was
539 performed manually. Basic genomic classifications—such as exon, intron, and intergenic
540 regions—were straightforward to assign. Similarly, regulatory annotations, including DNase
541 hypersensitive sites, transcription factor binding sites, and hyperdivergent regions, could be
542 systematically determined using existing datasets. However, annotating repetitive elements
543 within SVs was significantly more time-consuming. Many SVs overlapped repetitive
544 sequences that were not explicitly annotated by RepeatMasker, requiring manual inspection
545 of the variant and read sequences to deduce repeat structure.
546 In contrast, annotation of SVs in wild isolates was automated using GFF3-based
547 genome annotations. Variant calls were intersected with genomic features using *bedtools*
548 (Quinlan and Hall 2010), allowing for systematic classification. Automated annotation tools

549 such as *snpEff* (Cingolani et al. 2012) were not suitable for SV annotation, as they do not
550 properly account for the full extent of large structural variants. For example, an 8-kb deletion
551 may only be annotated at its breakpoints rather than across its entire span. To ensure
552 accurate functional classification, we assigned the highest-impact annotation observed
553 across the deleted region. If a deletion started upstream of a gene but extended into coding
554 sequences, it was annotated based on the most functionally significant feature it disrupted
555 (e.g., an exon rather than an upstream region).
556 Short variants (SNPs and small indels) in both MA and wild isolates were annotated
557 using *snpEff* with the following flags: -no-downstream -no-upstream -no-utr. As a result,
558 upstream, downstream, and UTR annotations were instead categorized as intergenic,
559 maintaining consistency with our SV annotation approach. *snpEff* produces a diverse set of
560 annotations, many of which are redundant or overly specific for our purposes. To
561 standardize annotation categories, we applied a systematic simplification approach using a
562 predefined mapping (**Supplementary Table 5**). This mapping condensed detailed
563 annotation labels into a manageable number of biologically meaningful categories, ensuring
564 consistency across variant types.
565
566 *Estimating the relative strength of selection for different categories of mutations*
567 To estimate the relative strength of selection, analogous to the dN/dS analysis, we first
568 defined a neutral class of variants. This neutral class comprises intergenic SNPs, intronic
569 SNPs, and synonymous substitutions within exons. We included intronic and intergenic
570 variants alongside synonymous variants to increase the sample size of MA variants in the
571 neutral class, given the limited number of synonymous MA variants in our dataset (only 14
572 observed). To reflect the expanded definition of the neutral class — which includes
573 intergenic and intronic variants alongside synonymous mutations — we refer to our
574 approach as the dN/dS* analysis.
575 To calculate the relative strength of selection for a particular class of mutation (e.g.,
576 structural variants in exons), we used the following formula:

577

578 $$dN\ /\ dS = \frac{\left(\frac{\#\ segregating\ variants\ in\ the\ focal\ class}{\#\ segregating\ variants\ in\ the\ neutral\ class}\right)}{\left(\frac{\#\ spontaneous\ mutations\ in\ the\ focal\ class}{\#\ spontaneous\ mutations\ in\ the\ neutral\ class}\right)}$$

579

580 This approach quantifies the relative diversity within a particular class of mutation against the
581 diversity in neutral classes after accounting for the mutation rates in both categories (data
582 obtained from spontaneous variants). Mutation counts for each category in the wild isolate
583 and MA populations are provided in **Table 3**.

584

585 *Simulation of Reference Genomes and Estimation of False Negative Rates*

586 To evaluate the sensitivity of our variant calling pipeline, we simulated structural variants in
587 the *C. elegans* reference genome (WS270) using the R package *RSVSim* (Bartenhagen and
588 Dugas 2013). For each variant type—insertions, deletions, and inversions—we generated
589 three independent simulated genomes. Within each variant type, we introduced 100 variants
590 of lengths 100 bp, 1,000 bp, and 10,000 bp, as well as 50 variants of 100,000 bp.

591 Following simulation, we applied our variant calling pipeline to assess recall rates.
592 Introducing structural variants into the reference genome shifts the positions of subsequent
593 variants, making direct locus-based comparisons dependent on tracking the precise order of
594 variant introduction. While this could be addressed if the software explicitly recorded variant
595 placement order, doing so would introduce additional dependencies into the analysis. To
596 avoid this complexity, we instead used a size-based evaluation approach, considering a
597 variant correctly detected if its length fell within predefined tolerance ranges: (98–102) bp,
598 (995–1,005) bp, (9,995–10,005) bp, and (99,995–100,005) bp for their respective size
599 categories. This approach simplified the evaluation while providing a systematic estimate of
600 false negative rates.

601

602 **Data Analysis**

603 All statistical analyses (e.g., Kolmogorov-Smirnov test, Fisher's exact test) were performed
604 in Python using SciPy (Virtanen et al. 2020). Data visualization was conducted using
605 Matplotlib (Hunter 2007) and Seaborn (Waskom 2021).
606

607 **Acknowledgments**

608 We thank Tim Crombie, Joanna Dembek, Lindsay Johnson, and Mike Snyder for assistance
609 in the lab, and Erik Andersen and Annalise Paaby for providing the wild isolate data. This
610 study was supported by the NIH award GM10722.
611

612 **Declaration of interests**

613 The authors declare no competing interests. A.S. contributed to this article in his personal
614 capacity as a graduate student at the University of Florida, and the views expressed do not
615 necessarily represent the views of Regeneron Pharmaceuticals Inc.
616

617 **Data availability**

618 Raw sequence data generated in this study are archived in the NCBI Short Read Archive -
619 PRJNA1233366. We also utilized publicly available data from C. elegans wild isolates from
620 the following SRA repositories (PRJNA523481, and PRJNA1025857). All code used for
621 structural variant (SV) calling, variant annotation, and manuscript figure generation is
622 available at https://github.com/Baer-Lab/c_elegans_spontaneous_sv.
623

624 **Figure Legends**

625 **Figure 1.** Schematic diagram of the mutation accumulation (MA) experiment. A
626 cryopreserved sample of the ancestor (N2 or PB306) was thawed onto an agar plate (G0,
627 left) and grown for a few days until the cryopreserved worms had reached the L4 larval
628 stage. L4-stage worms were transferred singly to new NGM agar plates; those were the
629 founders of the MA lines (MA.1, MA.2,...MA.n; n=100). At four-day intervals (one
630 generation), a single immature worm was picked at random onto a new plate. This

631 procedure was repeated until the experiment reached Gmax=250 generations. Individual
632 MA lines experienced fewer than Gmax generations, G(ave)=238 generations. The different
633 colored worms represent (the set of) unique mutations fixed in each MA line, which
634 contribute to the among-line (mutational) variance.
635
636 **Figure 2.** Recall rates by genotype, SV type, and SV size. N2 has the highest recall rate
637 across SV types and sizes. Small deletions (100 bp) have the highest recall rates,
638 comparable to 1-kb and 10-kb deletions. Recall rates of insertions drop sharply beyond 100
639 bp. Recall rate decreases with increasing SV size and genetic divergence from N2, a trend
640 also observed in PB306-derived MA lines (not shown). Inversions have the lowest recall
641 rates. QX1211, the most divergent genotype from N2, is the most challenging for SV
642 detection.
643
644 **Figure 3.** Distribution of SVs within and among chromosomes in wild isolates (density shown
645 in blue) and MA lines (vertical black lines). The overall distributions between these two
646 groups are not significantly different (Kolmogorov-Smirnov test; See text for details).
647
648 **Figure 4.** (Top) A schematic representation of the variants identified at the locus (I:
649 1567493) in the pedigree of MA lines. PBSV initially classified the 1.9 kb insertion and the
650 3.1 kb insertion as two independent mutations. However, a deeper analysis—accounting for
651 sequencing errors—reveals that a 1.2 kb segment was deleted within the inserted sequence
652 in the ancestor, leading to the observed 1.9 kb insertion.
653 (Bottom) IGV snapshot of the 1.2 kb deletion in PB306-derived MA 445. The IGV snapshot
654 shows pseudo-read alignments, which are assembled contigs representing longer
655 sequences. Some pseudo-reads fail to fully capture the inserted segment and appear as
656 soft-clipped sequences. If the inserted segment is not entirely covered within the pseudo-
657 read, it is clipped from the alignment, appearing as base calls (colored bars) instead of clean
658 (gray bars), fully aligned sequences. Some insertion sequences are misaligned because of

659 the repetitive nature of the locus; however, all pseudo-reads carry the

660 insertion. **Supplementary Figure S6** presents the same analysis using error-prone PacBio

661 raw reads.

662

663 **References**

664 Andersen EC, Gerke JP, Shapiro JA, Crissman JR, Ghosh R, Bloom JS, Felix MA, Kruglyak L. 2012.
665 Chromosome-scale selective sweeps shape Caenorhabditis elegans genomic diversity.
666 Nature Genetics 44:285-U283.
667 Audano PA, Sulovari A, Graves-Lindsay TA, et al. 2019. Characterizing the major structural variant
668 alleles of the human genome. Cell 176:663-+.
669 Baer CF, Phillips N, Ostrow D, Avalos A, Blanton D, Boggs A, Keller T, Levy L, Mezerhane E. 2006.
670 Cumulative effects of spontaneous mutations for fitness in Caenorhabditis: Role of
671 genotype, environment and stress. Genetics 174:1387-1395.
672 Baer CF, Shaw F, Steding C, et al. 2005. Comparative evolutionary genetics of spontaneous mutations
673 affecting fitness in rhabditid nematodes. Proceedings of the National Academy of Sciences of
674 the United States of America 102:5785-5790.
675 Bartenhagen C, Dugas M. 2013. RSVSim: an R/Bioconductor package for the simulation of structural
676 variations. Bioinformatics 29:1679-1681.
677 Barton NH. 1990. Pleiotropic models of quantitative variation. Genetics 124:773-782.
678 Bateman JR, Johnson JE. 2022. Altering enhancer-promoter linear distance impacts promoter
679 competition in cis and in trans. Genetics 222.
680 Beyter D, Ingimundardottir H, Oddsson A, et al. 2021. Long-read sequencing of 3,622 Icelanders
681 provides insight into the role of structural variants in human diseases and other traits.
682 Nature Genetics 53:779-+.
683 Böndel KB, Kraemer SA, Samuels T, McClean D, Lachapelle J, Ness RW, Colegrave N, Keightley PD.
684 2019. Inferring the distribution of fitness effects of spontaneous mutations in
685 *Chlamydomonas reinhardtii*. PLoS Biology 17:e3000192.
686 Boyle EA, Li YI, Pritchard JK. 2017. An Expanded View of Complex Traits: From Polygenic to
687 Omnigenic. Cell 169:1177-1186.
688 Chaisson MJ, Tesler G. 2012. Mapping single molecule sequencing reads using basic local alignment
689 with successive refinement (BLASR): application and theory. Bmc Bioinformatics 13:238.
690 Chaisson MJP, Wilson RK, Eichler EE. 2015. APPLICATIONS OF NEXT-GENERATION SEQUENCING
691 Genetic variation and the de novo assembly of human genomes. Nature Reviews Genetics
692 16:627-640.
693 Cingolani P, Platts A, Wang LL, Coon M, Nguyen T, Wang L, Land SJ, Lu XY, Ruden DM. 2012. A
694 program for annotating and predicting the effects of single nucleotide polymorphisms,
695 SnpEff: SNPs in the genome of Drosophila melanogaster strain w(1118); iso-2; iso-3. Fly 6:80-
696 92.
697 Collins RL, Brand H, Karczewski KJ, et al. 2020. A structural variation reference for medical and
698 population genetics. Nature 581:444-+.
699 Conrad DF, Pinto D, Redon R, et al. 2010. Origins and functional impact of copy number variation in
700 the human genome. Nature 464:704-712.
701 Crombie TA, Rajaei M, Saxena AS, Johnson LM, Saber S, Tanny RE, Ponciano JM, Andersen EC, Zhou J,
702 Baer CF. 2024. Direct inference of the distribution of fitness effects of spontaneous
703 mutations from recombinant inbred *Caenorhabditis elegans* mutation accumulation lines.
704 Genetics 228.
705 Denver DR, Morris K, Streelman JT, Kim SK, Lynch M, Thomas WK. 2005. The transcriptional
706 consequences of mutation and natural selection in Caenorhabditis elegans. Nature Genetics
707 37:544-548.
708 Diesh C, Stevens GJ, Xie P, et al. 2023. JBrowse 2: a modular genome browser with views of synteny
709 and structural variation. Genome Biology 24:74.
710 Eyre-Walker A, Keightley PD. 2007. The distribution of fitness effects of new mutations. Nature
711 Reviews Genetics 8:610-618.
712 Fisher RA. 1922. On the Dominance Ratio. Proceedings of the Royal Society of Edinburgh 42:321-341.

713 Friedman LS, Ostermeyer EA, Szabo CI, Dowd P, Lynch ED, Rowell SE, King MC. 1994. CONFIRMATION
714 OF BRCA1 LAY ANALYSIS OF GERMLINE MUTATIONS LINKED TO BREAST AND OVARIAN-
715 CANCER IN 10 FAMILIES. Nature Genetics 8:399-404.
716 Gilbert KJ, Zdraljevic S, Cook DE, Cutter AD, Andersen EC, Baer CF. 2021. The distribution of
717 mutational effects on fitness in *Caenorhabditis elegans* inferred from standing genetic
718 variation. Genetics 220.
719 Harvey WT, Ebert P, Ebler J, et al. 2023. Whole-genome long-read sequencing downsampling and its
720 effect on variant-calling precision and recall. Genome Research 33:2029-2040.
721 Hénault M, Marsit S, Charron G, Landry CR. 2024. The genomic landscape of transposable elements
722 in yeast hybrids is shaped by structural variation and genotype-specific modulation of
723 transposition rate. Elife 12.
724 Hunter JD. 2007. Matplotlib: A 2D Graphics Environment. Computing in Science & Engineering 9:90-
725 95.
726 Hurles ME, Dermitzakis ET, Tyler-Smith C. 2008. The functional impact of structural variation in
727 humans. Trends in Genetics 24:238-245.
728 James J, Kastally C, Budde KB, González-Martínez SC, Milesi P, Pyhäjärvi T, Lascoux M. 2023. Between
729 but not within species variation in the Distribution of Fitness Effects. Mol Biol Evol 13.
730 Karayiorgou M, Simon TJ, Gogos JA. 2010. 22q11.2 microdeletions: linking DNA structural variation
731 to brain dysfunction and schizophrenia. Nature Reviews Neuroscience 11:402-416.
732 Kim BY, Huber CD, Lohmueller KE. 2017. Inference of the Distribution of Selection Coefficients for
733 New Nonsynonymous Mutations Using Large Samples. Genetics 206:345-361.
734 Kimura M. 1962. On probability of fixation of mutant genes in a population. Genetics 47:713-719.
735 Kondrashov AS, Turelli M. 1992. Deleterious mutations, apparent stabilizing selection and the
736 maintenance of quantitative variation. Genetics 132:603-618.
737 Kondrashov FA, Ogurtsov AY, Kondrashov AS. 2006. Selection in favor of nucleotides G and C
738 diversifies evolution rates and levels of polymorphism at mammalian synonymous sites.
739 Journal of Theoretical Biology 240:616-626.
740 Konrad A, Flibotte S, Taylor J, Waterston RH, Moerman DG, Bergthorsson U, Katju V. 2018.
741 Mutational and transcriptional landscape of spontaneous gene duplications and deletions in
742 *Caenorhabditis elegans*. Proceedings of the National Academy of Sciences 115:7386-7391.
743 Koren S, Walenz BP, Berlin K, Miller JR, Bergman NH, Phillippy AM. 2017. Canu: scalable and accurate
744 long-read assembly via adaptive k-mer weighting and repeat separation. Genome
745 Research 27:722-736.
746 Kousathanas A, Keightley PD. 2013. A comparison of models to Infer the distribution of fitness
747 effects of new mutations. Genetics 193:1197-1208.
748 Lee D, Zdraljevic S, Stevens L, et al. 2021. Balancing selection maintains hyper-divergent haplotypes
749 in Caenorhabditis elegans. Nat Ecol Evol 5:794-807.
750 Li H. 2018. Minimap2: pairwise alignment for nucleotide sequences. Bioinformatics 34:3094-3100.
751 López-Cortegano E, Chebib J, Jonas A, Vock A, Künzel S, Keightley PD, Tautz D. 2025. The rate and
752 spectrum of new mutations in mice inferred by long-read sequencing. Genome Res 35:43-
753 54.
754 Lopez-Cortegano E, Craig RJ, Chebib J, Balogun EJ, Keightley PD. 2023. Rates and spectra of de novo
755 structural mutations in Chlamydomonas reinhardtii. Genome Research 33:45-60.
756 Lynch M, Hill WG. 1986. Phenotypic evolution by neutral mutation. Evolution 40:915-935.
757 Marshall CR, Noor A, Vincent JB, et al. 2008. Structural variation of chromosomes in autism spectrum
758 disorder. American Journal of Human Genetics 82:477-488.
759 Meyerson M, Pellman D. 2011. Cancer Genomes Evolve by Pulverizing Single Chromosomes. Cell
760 144:9-10.
761 Nattestad M, Goodwin S, Ng K, et al. 2018. Complex rearrangements and oncogene amplifications
762 revealed by long-read DNA and RNA sequencing of a breast cancer cell line. Genome
763 Research 28:1126-1135.

764 Nattestad M, Schatz MC. 2016. Assemblytics: a web analytics tool for the detection of variants from
765 an assembly. Bioinformatics 32:3021-3023.
766 Noyes MD, Harvey WT, Porubsky D, et al. 2022. Familial long-read sequencing increases yield of
767 de novo mutations. American Journal of Human Genetics 109:631-646.
768 Nurk S, Koren S, Rhie A, et al. 2022. The complete sequence of a human genome. Science 376:44-+.
769 Payer LM, Steranka JP, Yang WR, Kryatova M, Medabalimi S, Ardeljan D, Liu CH, Boeke JD,
770 Avramopoulos D, Burns KH. 2017. Structural variants caused by Alu insertions are associated
771 with risks for many human diseases. Proceedings of the National Academy of Sciences of the
772 United States of America 114:E3984-E3992.
773 Pinto DPagnamenta ATKlei L, et al. 2010. Functional impact of global rare copy number variation in
774 autism spectrum disorders. Nature 466:368-372.
775 Quinlan AR, Hall IM. 2010. BEDTools: a flexible suite of utilities for comparing genomic features.
776 Bioinformatics 26:841-842.
777 Rajaei M, Saxena AS, Johnson LM, Snyder MC, Crombie TA, Tanny RE, Andersen EC, Joyner-Matos J,
778 Baer CF. 2021. Mutability of mononucleotide repeats, not oxidative stress, explains the
779 discrepancy between laboratory-accumulated mutations and the natural allele-frequency
780 spectrum in *C. elegans*. Genome Research 31:1602-1613.
781 Robinson JT, Thorvaldsdóttir H, Wenger AM, Zehir A, Mesirov JP. 2017. Variant Review with the
782 Integrative Genomics Viewer. Cancer Research 77:e31-e34.
783 Rockman MV, Kruglyak L. 2009. Recombinational Landscape and Population Genomics of
784 Caenorhabditis elegans. Plos Genetics 5.
785 Sanders SJ, Ercan-Sencicek AG, Hus V, et al. 2011. Multiple Recurrent De Novo CNVs, Including
786 Duplications of the 7q11.23 Williams Syndrome Region, Are Strongly Associated with Autism.
787 Neuron 70:863-885.
788 Saxena AS, Salomon MP, Matsuba C, Yeh SD, Baer CF. 2019. Evolution of the mutational process
789 under relaxed selection in *Caenorhabditis elegans*. Molecular Biology and Evolution 36:239-
790 251.
791 Sedlazeck FJ, Rescheneder P, Smolka M, Fang H, Nattestad M, von Haeseler A, Schatz MC. 2018.
792 Accurate detection of complex structural variations using single-molecule sequencing.
793 Nature Methods 15:461-468.
794 Stiernagle T. 2006. Maintenance of *C. elegans*. In: T*Ce*R Community, editor. WormBook.
795 Stransky N, Cerami E, Schalm S, Kim JL, Lengauer C. 2014. The landscape of kinase fusions in cancer.
796 Nature Communications 5.
797 Tataru P, Mollion M, Glemin S, Bataillon T. 2017. Inference of Distribution of Fitness Effects and
798 Proportion of Adaptive Substitutions from Polymorphism Data. Genetics 207:1103-1119.
799 Virtanen PGommers ROliphant TE, et al. 2020. SciPy 1.0: fundamental algorithms for scientific
800 computing in Python. Nature Methods 17:261-272.
801 Walsh T, McClellan JM, McCarthy SE, et al. 2008. Rare structural variants disrupt multiple genes in
802 neurodevelopmental pathways in schizophrenia. Science 320:539-543.
803 Wang QL, Dhindsa RS, Carss K, et al. 2021. Rare variant contribution to human disease in 281,104 UK
804 Biobank exomes. Nature 597:527-+.
805 Waskom ML. 2021. seaborn: statistical data visualization. Journal of Open Source Software 6:3021.
806 Weiss LA, Shen YP, Korn JM, et al. 2008. Association between microdeletion and microduplication at
807 16p11.2 and autism. New England Journal of Medicine 358:667-675.
808 Wenger AM, Peluso P, Rowell WJ, et al. 2019. Accurate circular consensus long-read sequencing
809 improves variant detection and assembly of a human genome. Nature Biotechnology
810 37:1155-1162.
811 Wooster R, Bignell G, Lancaster J, et al. 1995. IDENTIFICATION OF THE BREAST-CANCER
812 SUSCEPTIBILITY GENE BRCA2. Nature 378:789-792.
813 Yi K, Ju YS. 2018. Patterns and mechanisms of structural variations in human cancer. Experimental
814 and Molecular Medicine 50.

815 Zhou X, Pan J, Wang YH, Lynch M, Long HA, Zhang Y. 2023. De Novo structural variations of
816 *Escherichia coli* detected by Nanopore long-read sequencing. Genome Biology and Evolution
817 15.

818

819

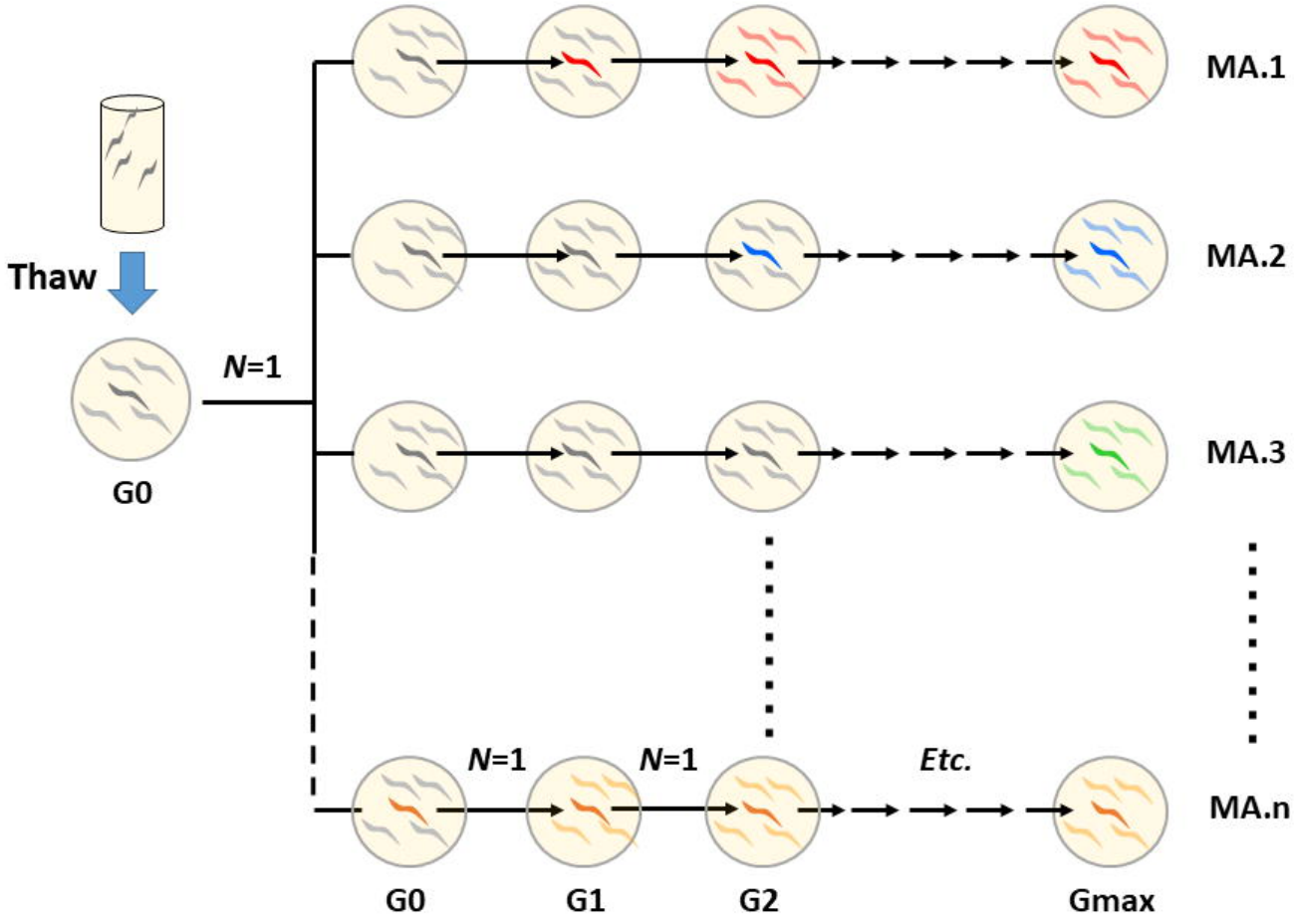
Thaw
G0
N=1
MA.1
MA.2
MA.3
MA.n
N=1
N=1
Etc.
G0
G1
G2
Gmax

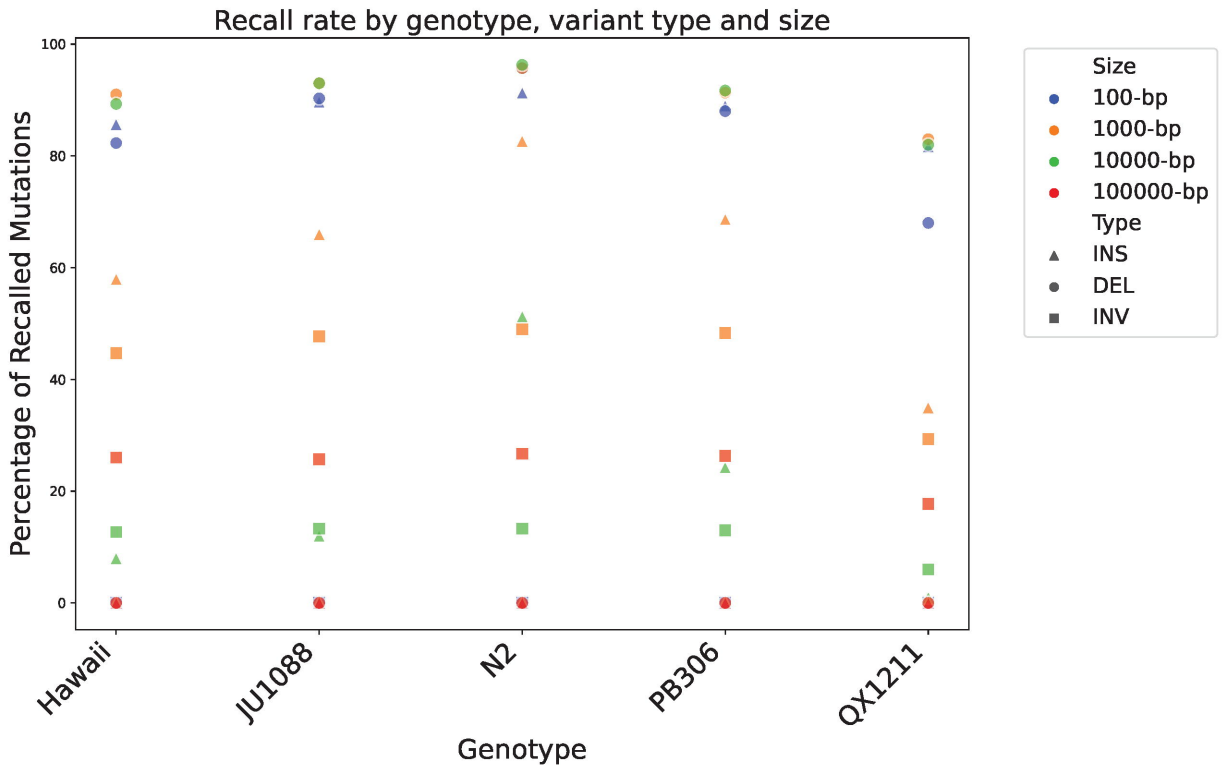
Recall rate by genotype, variant type and size
Percentage of Recalled Mutations
100
80
60
40
20
0
Hawaii
JU1088
N2
PB306
QX1211
Genotype
Size
100-bp
1000-bp
10000-bp
100000-bp
Type
INS
DEL
INV

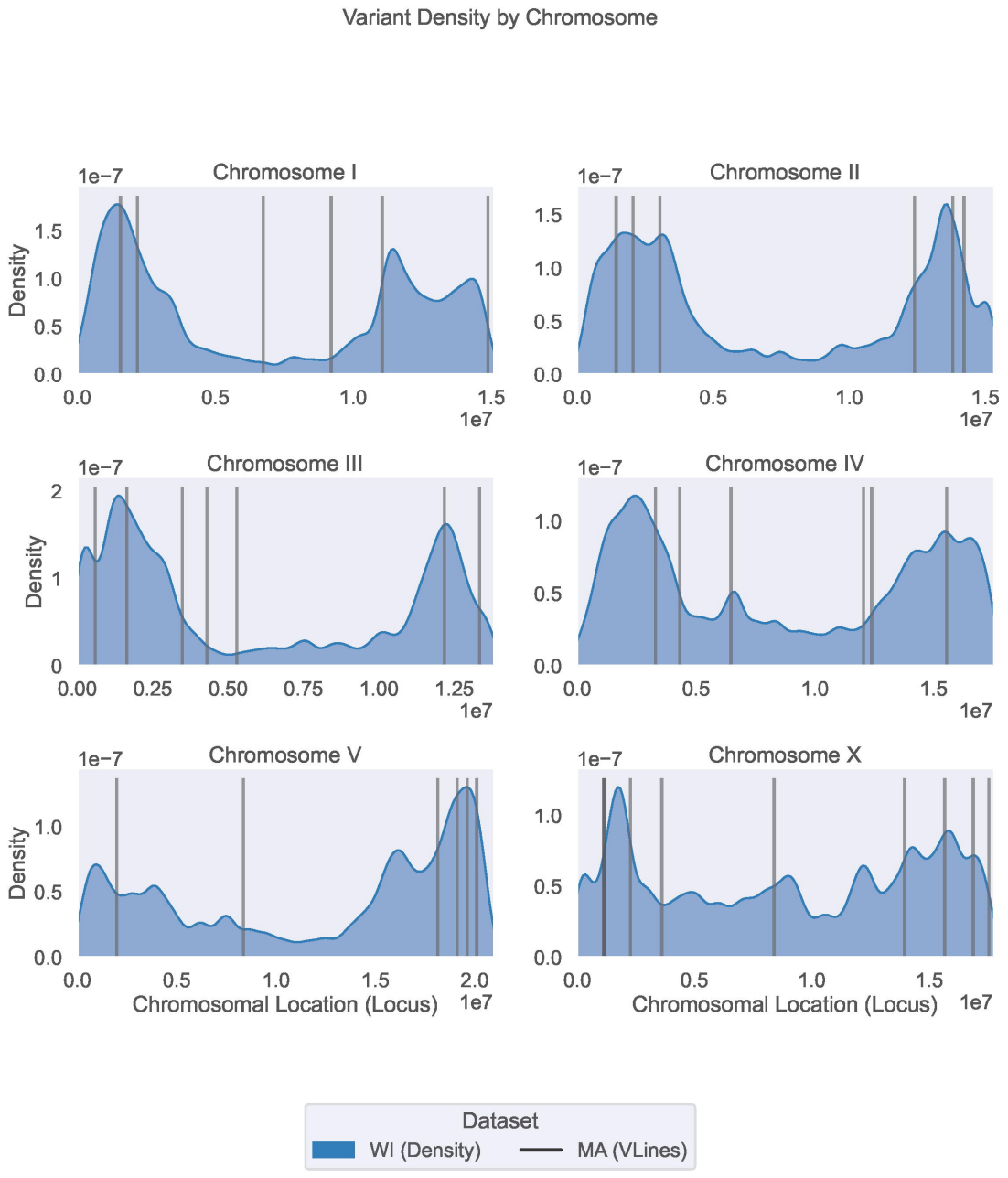
Variant Density by Chromosome
Chromosome I
Chromosome II
Chromosome III
Chromosome IV
Chromosome V
Chromosome X
1e−7
Density
1e7
Chromosomal Location (Locus)
Dataset
WI (Density)
MA (VLines)

(a)

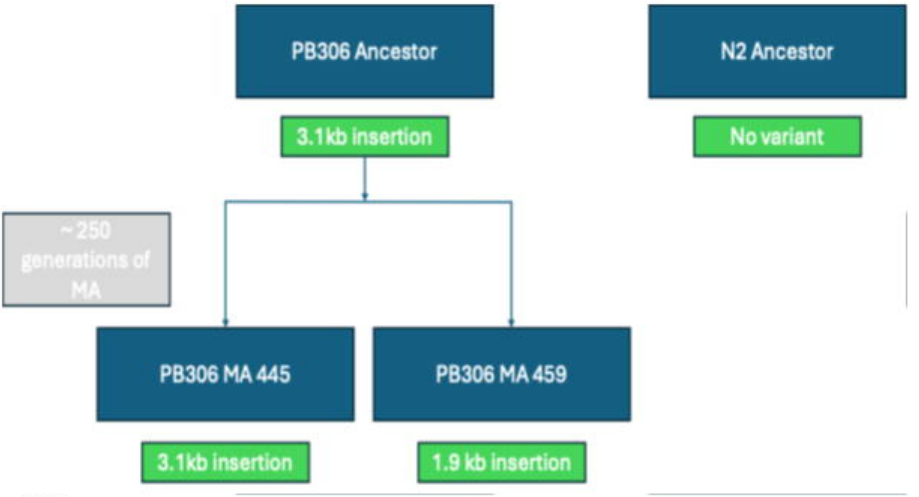
PB306 Ancestor
N2 Ancestor
3.1kb insertion
No variant
~250 generations of MA
PB306 MA 445
PB306 MA 459
3.1kb insertion
1.9 kb insertion

(b)

PB445 Coverage
PB459 Coverage
PB306 Coverage
N2 Coverage